Mutational Analysis of the Connector Segment in the HAMP Domain of Tsr, the *Escherichia coli* Serine Chemoreceptor[▽]

Peter Ames, Qin Zhou, and John S. Parkinson*

Biology Department, University of Utah, Salt Lake City, Utah 84112

HAMP domains are ~50-residue motifs, found in many bacterial signaling proteins, that consist of two amphiphilic helices joined by a nonhelical connector segment. The HAMP domain of Tsr, the serine chemoreceptor of *Escherichia coli*, receives transmembrane input signals from the periplasmic serine binding domain and in turn modulates output signals from the Tsr kinase control domain to elicit chemotactic responses. We created random amino acid replacements at each of the 14 connector residues of Tsr-HAMP to identify those that are critical for Tsr function. In all, we surveyed 179 connector missense mutants and identified three critical residues (G235, L237, and I241) at which most replacements destroyed Tsr function and another important residue (G245) at which most replacements impaired Tsr function. The region surrounding G245 tolerated 1-residue deletions and insertions of up to 10 glycines, suggesting a role as a relatively nonspecific, flexible linker. The critical connector residues are consistent with a structural model of the Tsr-HAMP domain based on the solution structure of an isolated thermophile HAMP domain (M. Hulko, F. Berndt, M. Gruber, J. U. Linder, V. Truffault, A. Schultz, J. Martin, J. E. Schultz, A. N. Lupas, and M. Coles, Cell 126:929–940, 2006) in which G235 defines a critical turn at the C terminus of the first helix and L237 and I241 pack against the helices, perhaps to stabilize alternative HAMP signaling conformations. Most I241 lesions locked Tsr signal output in the kinase-on mode, implying that this residue is responsible mainly for stabilizing the kinase-off signaling state. In contrast, lesions at L237 resulted in a variety of aberrant output patterns, suggesting a role in toggling output between signaling states.

Many signaling proteins in bacteria and archaea contain HAMP domains, a 50-residue motif named for its presence in histidine kinases, adenylyl cyclases, chemoreceptors known as methyl-accepting chemotaxis proteins (MCPs), and some phosphatases (8, 46). HAMP domains typically reside between the periplasmic sensing and cytoplasmic signaling regions of transmembrane proteins near the inner face of the cytoplasmic membrane and appear to play a central role in transmitting stimulus-induced conformational changes between the input and output domains of such signaling proteins. Their ability to mediate signaling transactions between heterologous input and output domains in chimeric proteins suggests that the mechanism of HAMP input-output control may be similar in diverse signaling proteins (6, 9, 25, 27, 42–44, 49). For example, in the hybrid Taz and Tez signaling proteins, the ligand binding domain of the aspartate chemoreceptor Tar controls the histidine kinase domain of EnvZ, an osmosensor, using either the Tar or EnvZ HAMP domain, respectively (43, 49). Although HAMP mutations have been characterized in a number of signaling proteins, the structure and function of HAMP domains remain poorly understood.

Chemoreceptors of the MCP family offer several experimental advantages for investigating the mechanisms of transmembrane signaling and HAMP-mediated input-output control (23). For example, the chemical effectors for *Escherichia coli* chemoreceptors are known, and several are small molecules that bind directly to the MCP periplasmic domain: Tar senses aspartate, and Tsr senses serine. Moreover, MCPs trigger fast stimulus response readouts: small changes in ligand concentration elicit large changes in the cell's flagellar rotation pattern with a latency of only a few hundred milliseconds. In spatial chemical gradients, these behavioral responses produce chemotactic migrations that can be easily monitored by colony size and morphology in soft agar medium. Unlike most other signaling proteins, a dedicated adaptation system adjusts the detection sensitivity and dynamic range of MCP chemoreceptors through reversible, feedback-controlled covalent modifications. Sensory adaptation allows the cells to make temporal comparisons of chemoeffector levels as they swim about and to adjust their sensitive detection range to match ambient chemoeffector levels.

Most importantly, a great deal is known about MCP structure and function (Fig. 1A). Native MCP molecules are homodimers of ~550-residue subunits organized into three functional modules: a transmembrane sensing module composed of a periplasmic ligand binding domain and four transmembrane helices, a signal-converting HAMP domain that adjoins one of the transmembrane helices in each subunit, and a four-helix bundle kinase control module connected to the HAMP domain (23). The kinase control portion of MCP molecules is highly conserved throughout the MCP superfamily (1). It typically contains several glutamic acid residues that are sites for adaptational modifications (methylation and demethylation), a flexible bundle segment with a glycine hinge, and a hairpin tip that interacts with other MCP molecules, with the histidine kinase CheA, and with CheW, a protein that couples CheA to receptor control.

The signaling behavior of an MCP molecule closely approx-

---

* Corresponding author. Mailing address: Biology Department, University of Utah, 257 South 1400 East, Salt Lake City, UT 84112. Phone: (801) 581-7639. Fax: (801) 581-4668. E-mail: parkinson@biology.utah.edu.
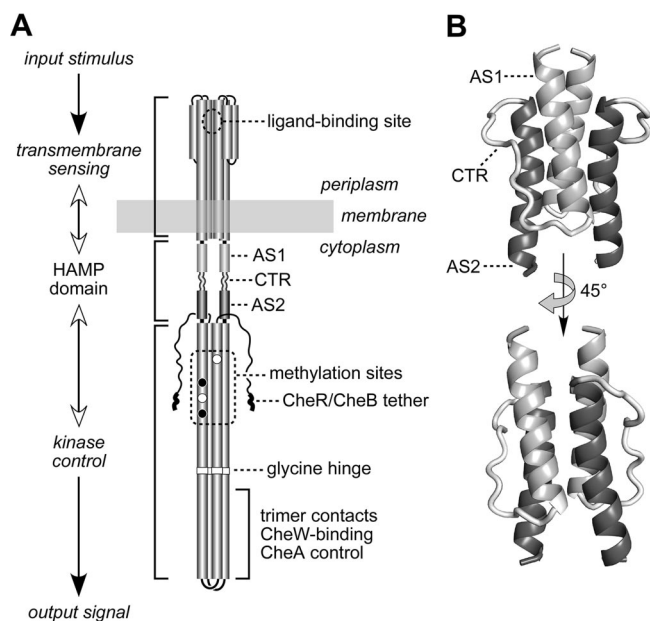
FIG. 1. (A) Functional architecture of Tsr and other MCP molecules. Native Tsr is a homodimer; each subunit is 551 residues in length. Most of the secondary structure elements are alpha-helices (shown as thickened cylinders). Structural elements of the TM sensing and kinase control domain are shown in their native arrangement; those of the HAMP domain are not. The kinase control domain is organized as a four-helix bundle of coiled coils. Several of the adaptation (methylation) sites are initially synthesized as glutamate residues (white circles); others are synthesized as glutamine residues (black circles) and subsequently converted to glutamates by an irreversible CheB-mediated deamidation. The C terminus of each subunit ends in a pentapeptide (NWETF) to which the adaptation enzymes CheR and CheB can bind. This tethering site is joined to the kinase control domain through a ~30-residue segment that is thought to serve as a flexible linker. (B) Structure of the Tsr-HAMP domain modeled on the Af1503-HAMP coordinates (24). HAMP connects to the TM helices at the top of the structure; its connection to the kinase control helices is at the bottom of the structure. Note that each connector segment interacts with the helices from the same subunit (most easily seen in the lower view). This shading convention (light gray, AS1; dark gray, AS2; black and white, CTR) is maintained in subsequent figures (Fig. 3, 6, and 7).

imates a two-state model (4, 13). Attractant-free MCPs activate the CheA kinase several hundredfold over basal levels, whereas attractant-occupied MCPs deactivate CheA. The cell's behavior reflects the proportions of receptor signaling complexes in each output state (designated kinase-on or clockwise [CW] and kinase-off or counterclockwise [CCW]). When chemical stimuli shift those proportions, the sensory adaptation system acts to restore the prestimulus balance, thereby poising the receptors for subsequent stimulus responses. The mechanisms of CheA activation and control by chemoreceptors are not yet understood at the molecular level but probably involve stimulus-induced changes in the stabilities of intra- and intersubunit interactions in the four-helix bundle, perhaps resulting in the stiffening or bending of the kinase control module (23).

The periplasmic sensing portions of Tar and Tsr have two symmetric, negatively cooperative ligand binding sites at the dimer interface. The binding of one ligand molecule to the

receptor dimer favors an asymmetric conformation characterized by an inward, ~2-Å displacement of one of the transmembrane segments adjoining the HAMP domain (18). HAMP converts this so-called piston motion into a symmetric conformational change that modulates receptor output through its connections to the kinase control subunits. These signaling events reflect concerted conformational changes throughout the receptor molecule. The adaptation sites interposed between HAMP and the kinase control segment at the cytoplasmic tip act as bidirectional conformational filters. Changes in the MCP methylation state influence not only the output kinase activity but also the transmembrane sensing module and, therefore, the intervening HAMP domain (28). Thus, the HAMP domains of MCPs probably have two discrete signaling conformations, under both stimulus and sensory adaptation control, that correspond to the CCW and CW output states of the kinase control module.

There is as yet no high-resolution structural information about the HAMP domains in MCP molecules. However, a cysteine-scanning study of Tar revealed that its HAMP domain contained two amphiphilic alpha-helical segments joined by a nonhelical connector (15). A recent in vivo cysteine-scanning analysis of the aerotaxis transducer Aer reached similar conclusions (45). Sequence analyses of HAMP segments in other signaling proteins indicate that the helix-connector-helix organization is most likely a universal feature of HAMP domains (8, 46). These predicted HAMP segments, particularly the helices, have many different designations in the literature. In this report, we use the designations AS1 and AS2 (amphipathic or amphiphilic sequences) and CTR (connector).

The recently determined high-resolution nuclear magnetic resonance structure of a HAMP domain isolated from a thermophile protein (Af1503) appears to be a good model for HAMP domains in general but particularly for those in MCPs (24). Despite few sequence identities between the HAMP domains of Tsr and Af1503, the primary structure of Tsr readily threads onto the Af1503 coordinates (Fig. 1B). The modeled structure is a dimeric, parallel, four-helix bundle, with each connector wrapped around the outsides of the helices from the same subunit. A similarly modeled structure for the HAMP domain in Tar was previously tested by cysteine-directed cross-linking in vitro (41). That study demonstrated intersubunit disulfide formation between AS1 and AS2 positions that were predicted to be in close contact by the Af1503-based structural model.

To gain deeper molecular insights into the in vivo structure and function of HAMP domains, we initiated a detailed mutational analysis of the HAMP domain in Tsr, the E. coli serine chemoreceptor. At the outset, we assumed that Tsr-HAMP had two alternative signaling conformations, corresponding to kinase-on and kinase-off output states. Our studies aimed to investigate the nature of those signaling states, how stimulus inputs and sensory adaptation interconvert them, and how they in turn control output activity. This report focuses on the connector segment. We determined the connector residues most critical for Tsr function, characterized the signal output patterns produced by various connector lesions, and identified a linker segment within the connector that tolerates multiresidue insertions. These new genetic features of the Tsr-HAMP connector fully support the premise that the

Af1503-HAMP structure closely corresponds to one of the in vivo Tsr-HAMP signaling states.

MATERIALS AND METHODS

Bacterial strains. All strains were derivatives of *E. coli* K-12 strain RP437 (34) and contained the following markers relevant to this study: UU1250 [Δ*aer-1* Δ*tsr-7028* Δ(*tar-tap*)*5201* Δ*trg-100*] (5), UU1535 [Δ*aer-1* Δ(*tar-cheB*)*2234* Δ*tsr-7028* Δ*trg-100*] (10), UU1615 [Δ*aer-1* Δ(*tar-tap*)*5201* Δ*trg-100*] (21), UU1623 [Δ(*tsr*)*7028* Δ*tap-3654* Δ*trg-100*] (this work), UU2377 [*tsr-R69E* Δ*aer-1* Δ(*tar-tap*)*5201* Δ*trg-4543* Δ*recA*-SstII/EcoRI] (this work), and UU2378 [*tsr-T156K* Δ*aer-1* Δ(*tar-tap*)*5201* Δ*trg-4543* Δ*recA*-SstII/EcoRI] (this work). The *tsr* mutations in UU2377 and UU2378 were introduced into the chromosome by a two-step allele replacement procedure (K. A. Datsenko and B. L. Wanner, personal communication).

Plasmids. Plasmids used in this work were pKG116, a derivative of pACYC184 (16) and pKMY297 (48) that confers chloramphenicol resistance and has a sodium salicylate-inducible expression/cloning site (14); pPA114, a relative of pKG116 that carries wild-type *tsr* under salicylate control (5); pRR48, a derivative of pBR322 (12) that confers ampicillin resistance and has an expression/cloning site with a *tac* promoter and an ideal (perfectly palindromic) *lac* operator under the control of a plasmid-encoded *lacI* repressor, inducible by isopropyl-β-D-thiogalactopyranoside (IPTG) (39); and pRR53, a derivative of pRR48 that carries wild-type *tsr* under IPTG control (39).

Directed mutagenesis. Plasmid mutations were generated by QuikChange PCR mutagenesis as previously described (5). For all-codon mutagenesis, we used oligonucleotide primer pools that were fully degenerate, i.e., had equal frequencies of the four bases A, C, G, and T at all three base positions of the targeted codon. Mutations were verified by sequencing the entire *tsr* coding region in the mutant plasmid.

Chemotaxis assays. Host strains carrying Tsr expression plasmids were assessed for chemotactic ability on tryptone soft agar plates (32) containing appropriate antibiotics (ampicillin [50 μg/ml] or chloramphenicol [12.5 μg/ml]) and inducers (IPTG or salicylate). Plates were incubated for 7 to 10 h at 30°C or 32.5°C.

Flagellar rotation assays. Flagellar rotation patterns of Tsr plasmid-containing cells were analyzed by antibody tethering as described previously (29). The overall percentage of time spent in CW rotation was calculated from the percentage of cells in each of five rotational categories (exclusively CCW, CCW reversing, balanced CCW-CW, CW reversing, and exclusively CW) as described previously (5). Rotational patterns were defined as follows based on the percent CW time caused by a Tsr plasmid in strains UU1535 and UU1250, respectively (CCW locked, ≤15%, ≤15%; CW locked, ≥70%, >75%; CCW biased, 16 to 69%, <25%; CW biased, ≥70%, 41 to 75%; bipolar, ≥70%, <15%; unbiased, ≥70%, 15 to 40%; inverted, <60%, >80%).

Expression levels of mutant Tsr proteins. Tsr expression from pRR53 and pPA114 derivatives was analyzed in strain UU1535 (to avoid multiple modification states) as described previously (2).

Protein modeling and structural display. Atomic coordinates for the Tsr-HAMP domain were generated from the Af1503-HAMP coordinates (PDB accession number 2ASW) by the Swiss-Model server (36). Structure images were prepared with MacPyMOL software (http://www.pymol.org).

RESULTS

Strategy for mutational analysis of the Tsr-HAMP connector. To identify the connector residues most critical for Tsr function, we carried out a codon-by-codon mutagenesis of the connector coding region in two *tsr* expression plasmids, pRR53 and pPA114, using degenerate PCR primers as detailed in Materials and Methods. At optimal inducer concentrations (100 μM IPTG or 0.6 μM Na salicylate, respectively), pRR53 and pPA114 confer wild-type Tsr function to UU1250, a host strain carrying deletions of all five *E. coli* MCP family genes (*tsr*, *tar*, *tap*, *trg*, and *aer*). Candidate mutant plasmids were tested in strain UU1250 for Tsr function at optimal induction conditions on tryptone soft agar plates. Representative examples of the mutant phenotypes found are shown in Fig. 2. On the basis of these initial chemotaxis tests, each mutant plasmid
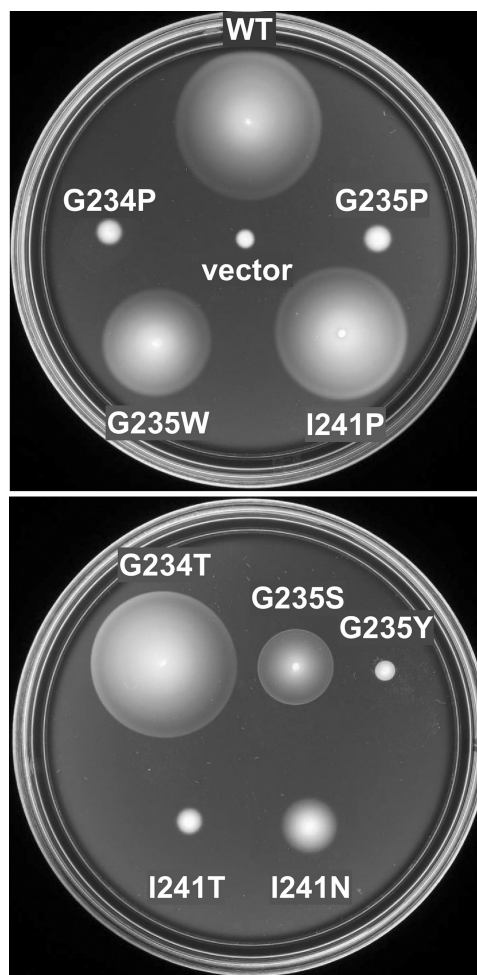

FIG. 2. Representative chemotaxis phenotypes of Tsr-HAMP connector mutants. Tryptone soft agar plates were toothpick inoculated from fresh transformant colonies of UU1250 cells carrying pRR53 (wild-type Tsr), its mutant derivatives, or pRR48 (vector control). Plates contained 50 μg/ml ampicillin and were incubated at 32.5°C for 8 h. The outer (serine) ring of the G235W and I241P colonies has a wild-type morphology, whereas that of the G234T mutant has a thinner, sharper edge. The G235S and G235Y colonies also have sharp edges, which are indicative of some chemotactic ability. The I241T and I241N colonies form diffuse discs with a ring near their perimeter, most likely reflecting some residual chemotactic ability. In contrast, the G234P and G235P mutants exhibit a fully null phenotype. In UU1250, these mutant transducers produce both CCW and CW flagellar rotation (Fig. 4), which enables the cells to spread through the agar more readily than the vector-containing cells, which are CCW only.

was assigned to one of three functional categories: Tsr[+] (colony size and morphology very similar to wild-type, e.g., G235W and I241P in Fig. 2), Tsr^{+/−} (reduced colony size and/or nonwild ring morphology, e.g., G234T, G235S, G235Y, I241N, and I241T in Fig. 2), and Tsr[−] (complete loss of function, comparable to the vector control phenotype, e.g., G234P and G235P in Fig. 2).

Overview of the mutational scan. Our mutant hunt yielded an average of 13 nonwild amino acids at each of the 14 connector residues surveyed (G234 to N247) (Fig. 3). Although incomplete, the variety of amino acid replacements at each position was sufficient to identify the functionally critical con-
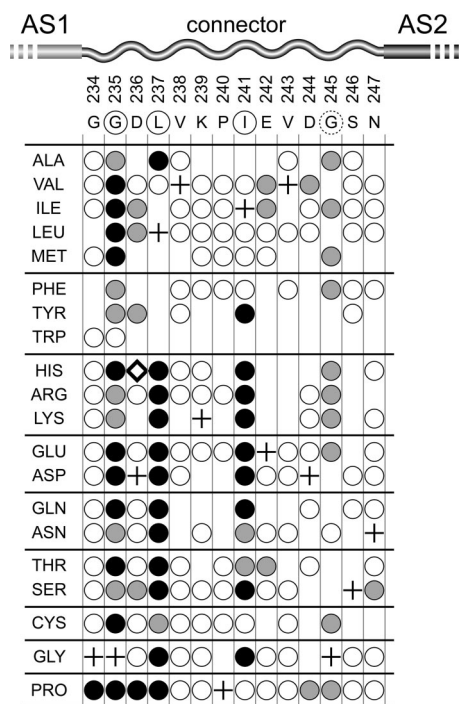
FIG. 3. Mutational survey of Tsr-HAMP connector residues. The mutations isolated at each position and their phenotypes are indicated by circles: white, Tsr+; gray, Tsr+/−; black, Tsr−. See the text for an explanation of these phenotypes. Plus symbols indicate the wild-type residues. Where no symbol is given, that particular replacement was not isolated. The D236H mutant protein (open diamond) was poorly expressed or unstable (~14% of the wild-type steady-state level). All other mutant proteins were present at 50% or more of the wild-type level (data not shown). Amino acid replacements are grouped by side chain properties to facilitate comparisons among the sites. At the top, critical connector residues are circled: G235, L237, and I241. At these positions, a majority of replacements impaired function, and a majority of those were null defects. G245 (dashed circle) is a less critical site: a majority of replacements at this residue impaired function, but none of them caused null defects.

N247), suggesting that flexibility may be an important functional attribute of this segment.

The remainder of this report will focus exclusively on the characterization of the Tsr− connector mutants. Owing to their loss-of-function nature, we cannot be certain that the mutant proteins have native or near-native structures. However, at optimal induction conditions for wild-type Tsr, only one of the null mutants (D236H) exhibited a steady-state Tsr protein level below 50% of the wild-type (Fig. 3 and data not shown), which implies that the other 34 null mutant proteins have wild-type intracellular stabilities and, possibly, overall native structures as well. These 34 mutants were subjected to a variety of additional in vivo tests to elucidate the nature of their functional defects. The properties of the mutants are summarized in Table 1 and discussed in the following sections.

Steady-state output signals of the mutant receptors. Wild-type receptors exhibit two alternative signaling states (kinase-on or CW and kinase-off or CCW), which presumably reflect different conformations of their output-controlling HAMP domains. Chemical stimuli and reversible covalent modification at the methylation sites involved in sensory adaptation influence the equilibrium proportions of the CW and CCW signaling states. Attractant binding favors the CCW state; subsequent methylation increases shift receptors to the CW state to bring about sensory adaptation. The adaptation process is controlled at two levels, through state-dependent differences in the substrate properties of receptor molecules (CCW receptors are good substrates for the methyltransferase CheR, and CW receptors are good substrates for the methylesterase CheB) and through feedback phosphorylation control of CheB activity.

The cell's pattern of flagellar rotation reflects the interplay between excitatory and adaptational signaling by its receptors. To classify the signal output states of mutant receptors, we observed the flagellar rotation patterns that they produced in antibody-tethered cells under unstimulated, steady-state conditions. We compared signal outputs in two different hosts, UU1250, which is adaptation competent, and UU1535, a closely related strain that lacks the CheR and CheB adaptation enzymes. Tsr molecules are initially synthesized with a QEQE pattern at the four major methylation sites. The glutamine residues mimic glutamyl methyl esters, the methylated form, but can be converted to glutamates, the unmethylated form, by irreversible CheB-mediated deamidation. Thus, in UU1535, unmodified Tsr molecules retain a QEQE modification pattern, which produces strongly CW-biased signal output in wild-type Tsr (Fig. 4, inset). Such cells spend over 80% of their time in CW rotation. In UU1250, the adaptation system adjusts wild-type Tsr molecules, through deamidation, methylation, and demethylation reactions, to a more CCW-biased signal output. The cells spend about 75% of their time in CCW rotation but with frequent reversals that correspond to the tumbling episodes seen in free-swimming cells (Fig. 4, inset). Thus, the rotation profile produced by a mutant receptor in UU1535 reflects its unmodified (QEQE) output state; its UU1250 rotation pattern indicates whether or not that output is subject to sensory adaptation control.

The 34 connector null lesions defined seven different output patterns (Fig. 4). At one extreme, some mutations produced exclusively CCW rotation in both UU1535 and UU1250. Mu-

nector residues and their important side chain characteristics. For example, nearly all null lesions (32/35 null lesions) involved only three residues (G235, L237, and I241) (Fig. 3). Moreover, most of the replacements at those three positions impaired or abrogated Tsr function (18/19 at G235, 13/14 at L237, and 11/17 at I241). These findings indicate that G235, L237, and I241 are the connector residues most critical for Tsr function. Proline replacements at G234 and D236 also caused null phenotypes, but few other changes at these positions impaired Tsr function (15/16 Tsr+ at G234 and 8/14 Tsr+ at D236). The uniquely deleterious consequences of the proline replacements suggest that backbone flexibility at these residues is more important to function than their side chain volume or chemical properties.

G245 also appeared to be a functionally important connector residue but less critical than G235, L237, and I241. Although no G245 replacements caused a null phenotype, 10/11 replacements at this position caused a partial loss of function. The native residues in this portion of the connector all have relatively small side chains (V243, D244, G245, S246, and

TABLE 1. Phenotypes of null Tsr-HAMP connector mutants

Residue	Amino acid replacement	Function in heterodimers[a]	Functional rescue by Tar[b]	Functional jamming of Tar[c]	Signal output[d]
G234	P	+/+	0	+	Bipolar
G235	C	0/0	0	++	CCW locked
	H, L, M, Q	0/0	0	+	CCW locked
	D, E	±/±	0	+	CW locked
	P	+/+	0	+	Unbiased
	I, T, V	+/+	0	+	Bipolar
D236	P	+/+	0	0	CW locked
L237	H	+/+	0	+	CCW locked
	K, N	+/+	0	+	CW locked
	E	+/+	0	+	Bipolar
	R	+/+	0	0	CW locked
	D, P, S	+/+	0	0	CCW biased
	G	+/+	0	0	Bipolar
	Q	+/+	0	0	Inverted
	A	+/+	0	0	CW biased
	T	+/+	++	0	CCW biased
I241	D, E, G, K, R	+/+	0	+	CW locked
	Y	+/+	0	+	CW biased
	Q	+/+	+	0	CW biased
	S	+/+	+	0	Bipolar
	H	+/+	+	+	CW biased

[a] Assessed by soft agar colony morphology in strains UU2377 and UU2378, respectively (Fig. 5). +/+, full Tsr function in both tester strains; ±/±, reduced Tsr function in both strains; 0/0, no Tsr function in either strain.
[b] Assessed by soft agar colony morphology in strain UU1623; ++, full Tsr function; +, partial Tsr function; 0, no Tsr function.
[c] Assessed by soft agar colony morphology in strain UU1623. ++, complete jamming (no Tar function); +, partial jamming (reduced Tar function at elevated Tsr* levels); 0, no jamming (full Tar function).
[d] Assessed by flagellar rotation patterns in strains UU1250 and UU1535 (Fig. 4).

tations at the other extreme produced very high rates of CW rotation in both hosts. We tentatively designate these as being "locked output" defects, but note that CW rotation depends on the assembly of receptor signaling complexes that activate CheA, whereas CCW rotation is the default direction of flagellar rotation. Thus, "CCW-locked" receptors could include ones that are simply defective in ternary complex assembly as well as ones that assemble ternary signaling complexes "locked" in the CCW (CheA-deactivating) output state. In any case, mutant receptors with locked signal outputs are, by definition, unresponsive to the sensory adaptation system. Such receptors could be either poor substrates for modification or insensitive to changes in modification state. The methylation patterns and ternary complex phenotypes of such mutant receptors will be addressed in a subsequent study.

Some mutant receptors exhibited adjustable output signals that were biased toward the kinase-off (CCW-biased) or kinase-on (CW-biased) states in strain UU1250. Both types of signal-biased receptors exhibited roughly wild-type output patterns in UU1535 (i.e., in the QEQE modification state) but aberrant output patterns in UU1250, where the sensory adaptation system was operational. Mutant receptors designated "bipolar" showed even more dramatic differences in signal output in the two host strains: extreme CW output in UU1535 and extreme CCW output in UU1250. The biased- and bipolar-output mutant receptors are evidently subject to adaptational modification and with the same output logic as that of wild-type receptors but with aberrant fine control over signal output.

One connector lesion (G235P) produced a wild-type output pattern. Although its signal output appeared to respond normally to the adaptation system, this mutant receptor did not mediate chemotaxis, suggesting that its output cannot be properly modulated by serine stimuli. One other mutant receptor (L237Q) exhibited an inverted output pattern in the two hosts. In UU1535, its output was moderately CCW, whereas in UU1250, its output was moderately CW.

Functional interactions with the aspartate receptor. To better understand the nature of the signaling defects in the Tsr connector mutants, we examined their behavioral effects in strain UU1623, which contains a wild-type aspartate receptor (Tar). Receptors of different types are known to form mixed signaling teams, most likely based on a trimer-of-dimers organization (2, 5, 33, 38, 39). In such mixed teams, wild-type Tar can functionally rescue some Tsr defects, and some Tsr defects can jam the function of their wild-type Tar partners. Many Tsr defects are neither functionally rescuable nor able to jam the signaling activities of other receptors. The Tsr-CTR* mutants fell into all three possible categories (Table 1). Eight mutant receptors (D236P, L237A, L237D, L237G, L237P, L237Q, L237R, and L237S) were neither rescuable nor jamming. In principle, their lesions might prevent trimer-of-dimer formation, but this seems unlikely, because the mutant receptors all exhibited some ability to activate CheA in flagellar rotation tests (Fig. 4 and Table 1). Several lines of evidence suggest that receptors must form a higher-order complex, most likely trimers of dimers, in order to assemble active ternary complexes (2, 3, 5, 11, 17, 19, 20, 31, 37, 40, 47). All other Tsr-CTR*
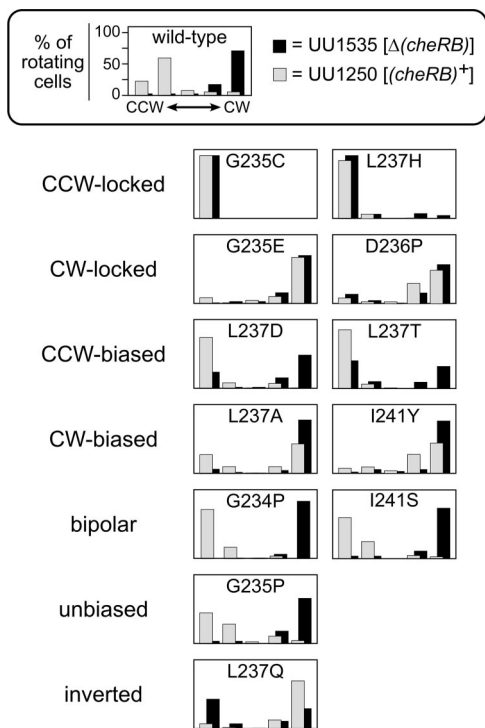
FIG. 4. Examples of signal output patterns of loss-of-function (null) Tsr-HAMP connector mutants. Mutant pRR53 derivatives were transferred to UU1535 (adaptation-defective) and UU1250 (adaptation-proficient), and their resultant flagellar rotation patterns were assessed by cell tethering. Each panel shows the rotation profile of 100 cells of each strain, distributed across five rotation classes, from exclusively CCW on the left through frequently reversing in the center to exclusively CW on the right. The wild-type pattern is shown at the top. The criteria used to define the various mutant output categories are described in Materials and Methods. Where two examples are given for an output class, they represent the most different patterns of that class.
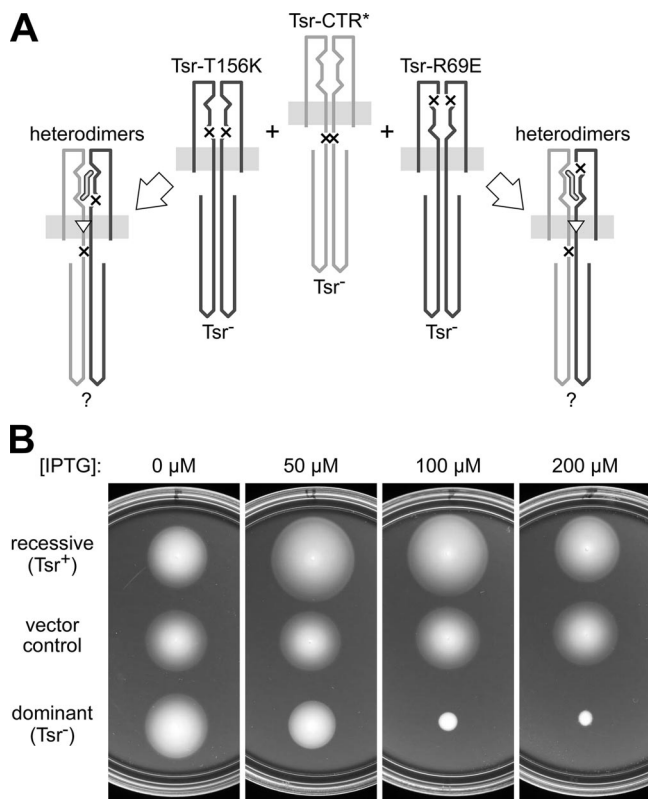

FIG. 5. (A) Scheme for testing dominance and signal asymmetry of Tsr-HAMP connector lesions. Plasmid-borne connector mutations were tested for Tsr function in host strains with a binding site defect (R69E or T156K) in their chromosomal *tsr* gene. The coexpression of both Tsr subunits leads to the formation of heterodimers that are competent for serine binding in one orientation. Recessive HAMP defects should allow those heterodimers to function; dominant HAMP defects should not. If the HAMP lesion affects signaling asymmetrically, one type of heterodimer could function, whereas the other does not. × symbols represent mutational lesions, S-shaped symbols represent serine molecules, and white triangles indicate the subunit that transmits the ligand-induced piston signal to the HAMP domain. (B) Examples of recessive and dominant Tsr-HAMP connector lesions. Tryptone soft agar plates containing 50 μg/ml ampicillin and various concentrations of IPTG were inoculated with freshly transformed colonies and incubated at 32.5°C for 8 h. The host strain was UU2377 (Tsr-R69E); plasmids were pRR48 (vector control) and pRR53 derivatives expressing Tsr-I241R (recessive) or Tsr-G235C (dominant). Note that the Tsr-R69E receptor, although defective in serine sensing, is able to mediate a slow migratory response, most likely via aerotaxis or pH taxis (22, 35). In combination with a recessive HAMP lesion (I241R), this behavior is supplanted by a more robust chemotactic response to serine (note differences in colony morphology at 50 or 100 μM IPTG). In combination with a dominant HAMP lesion (G235C), this behavior is suppressed, and the strain exhibits a null phenotype (e.g., 100 μM IPTG).

receptors were either rescuable, jamming, or both, implying that they are able to form mixed trimers of dimers with Tar. Three mutant receptors (L237T, I241Q, and I241S) were rescuable and nonjamming, 1 (I241H) was both rescuable and jamming, and 22 jammed Tar function but were not functionally rescuable (Table 1).

Dominance and functional asymmetry. The mutant Tsr receptors were initially scored for function as homodimers; i.e., both Tsr subunits contained the same connector lesion. To determine whether the HAMP connector segment might play a critical role in converting asymmetric piston inputs into symmetric conformational outputs, we tested the signaling properties of heterodimers that contained one mutant subunit (CTR*) and one wild-type subunit (CTR⁺). These tests were done by expressing CTR* subunits in Tsr mutant hosts with recessive serine binding defects so that neither of the homodimer species could support Tsr function. Heterodimers containing either the R69E or T156K lesion in one subunit have one functional serine binding site, but the subsequent piston displacement takes different routes (Fig. 5A). In R69E heterodimers, ligand-induced piston motions occur in the R69E subunit, whereas in T156K heterodimers, the piston displacement occurs in the opposite, CTR*, subunit. Connec-

tor lesions that are fully recessive should function in both configurations, whereas those that are fully dominant should function in neither configuration (see examples in Fig. 5B). In contrast, any connector lesions that disrupt input signals to HAMP might show functional asymmetry in these tests, for example, by blocking signal transmission in T156K heterodimers but not in R69E heterodimers. However, all of the Tsr-CTR* lesions exhibited symmetric behavior (Table 1 and data not shown): five mutant receptors (G235C, G235H,

AS1   connector   AS2

234 235 236 237 238 239 240 241 242 243 244 245 246 247

G (G) D (L) V K P (I) E V D (G) S N

turn | packing interactions? | linker

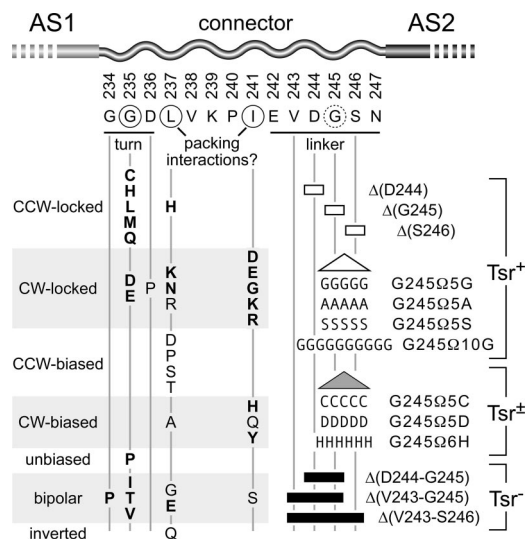|	turn	packing interactions?		linker		
CCW-locked	C H L M Q	H			□	Δ(D244)
					□	Δ(G245)
					□	Δ(S246)
CW-locked	D E	K N R	D E G K R	GGGGG	G245Ω5G	Tsr+
				AAAAA	G245Ω5A	
				SSSSS	G245Ω5S	
CCW-biased		D P S T		GGGGGGGGGG	G245Ω10G	
CW-biased		A	H Q Y	CCCCC	G245Ω5C	Tsr±
				DDDDD	G245Ω5D	
unbiased	P I T V			HHHHHH	G245Ω6H	
bipolar	P	G E Q	S	▬▬	Δ(D244-G245)	Tsr−
				▬▬▬	Δ(V243-G245)	
inverted				▬▬▬▬	Δ(V243-S246)	

FIG. 6. Structure-function features in the Tsr-HAMP connector. Critical and important residues are circled. Amino acid replacements that cause jamming behavior are shown in boldface type. The connector exhibits three subsegments with different inferred roles. G234 to D236 are small residues that may comprise a turn. Nearly every type of amino acid replacement at G235 destroys function. Most replacements at L237 and I241 also destroy Tsr function but with a variety of signal output patterns. These residues may contribute side chain packing interactions that stabilize alternative HAMP signaling conformations. The E242-to-N247 segment contains mostly small residues and may serve as a flexible linker. Single-residue deletions at position 244, 245, or 246 had no deleterious effect on Tsr function. Similarly, the indicated 5- and 10-residue insertions between G245 and S246 did not interfere with Tsr function. Other insertions and larger deletions in this segment impaired or destroyed Tsr function, respectively.

G235L, G235M, and G235Q) were dominant and failed to function in either binding site configuration, two others (G235D and G235E) exhibited partial complementation in both configurations, and the remainder were recessive, functioning well in both configurations (Table 1).

One potential complication in interpreting the heterodimer tests is the possibility that mutant homodimers could interfere with function by spoiling trimer-of-dimer receptor teams. Indeed, both the partially and fully dominant CTR* mutations exhibited strong jamming phenotypes as homodimers (Table 1). However, some recessive mutations were also strong jammers, so jamming effects are not strictly correlated with dominance. Moreover, the dominance tests were carried out at roughly comparable CTR*:CTR+ ratios to ensure that CTR*/ CTR* homodimers were at low relative levels.

A linker subsegment in the connector. With the exception of G245 (see above), Tsr function was impervious to amino acid replacements in connector residues 242 to 247 (Fig. 3). The residues in this segment have relatively small side chains (E, V, D, G, S, and N) and might serve as a relatively nonspecific flexible linker. To test this idea, we constructed various insertion and deletion mutations in this region. Several one-residue deletions (D244, G245, or S246) retained full wild-type function, but deletions of two or more residues in this segment abrogated Tsr function (Fig. 6). Moreover, insertions of 5 or 10 glycines, 5 alanines, or 5 serines between G245 and S246 had no deleterious effect on Tsr function (Fig. 6). In contrast,

insertions of five cysteine, five aspartate, or six histidine residues compromised Tsr function to different extents (Fig. 6). These results indicate that the length of the connector linker segment is close to the minimum needed for proper function but that longer segments do not impair function provided that they retain sufficient flexibility.

DISCUSSION

Structure-function features of the Tsr-HAMP connector. The principal findings of this study are summarized in Fig. 6. We identified three connector residues (G235, L237, and I241) at which most amino acid replacements abrogated Tsr function and another (G245) at which most replacements impaired function. These residues define three structural features with different functional roles in the connector segment.

G235 and its flanking neighbors, G234 and D236, all small residues, may comprise a turn. Proline replacements at any of these positions destroy function, suggesting that backbone flexibility is important in this region of the connector. However, other amino acid replacements are tolerated at G234 and D236; only the central G235, which is highly conserved in HAMP domains, is critical.

L237 and I241 were sensitive mainly to polar and charged amino acid replacements, but glycines and other small residues (A or S) at either position also destroyed function. This pattern suggests that hydrophobic side chains at these positions might stabilize HAMP signaling structures through packing interactions with other HAMP elements or other parts of the receptor molecule.

Except for the semicritical G245, the C-terminal portion of the connector (residues E242 to N247) was relatively impervious to amino acid replacements. The residues in this segment have relatively small side chains and probably serve as a flexible linker. This segment is one residue longer than the minimum needed for full signaling function but tolerates insertions of additional amino acids with small side chains (G, A, and S). However, insertions of cysteines or aspartates, also small residues, compromised function, presumably due to the special nature of their side chains, which could reduce backbone flexibility in a variety of ways. Conceivably, this linker plays a role in signaling-related HAMP conformational changes.

In vivo structure of Tsr-HAMP. The critical residues and structural features of the Tsr-HAMP connector deduced from our mutant analysis (Fig. 6) provide strong circumstantial support for the helix bundle model of Tsr-HAMP based on the Af1503-HAMP structure (24) (Fig. 7). Several lines of evidence suggest that this model closely resembles an in vivo structure of Tsr-HAMP.

The three functionally critical Tsr-HAMP connector residues (G235, L237, and I241) have prominent roles in the modeled structure (Fig. 7). The connector segment is an extended strand that makes a sharp hairpin turn at the C terminus of the AS1 helix. G235 is central to this turn (Fig. 7C). In the Tsr-HAMP model, the side chains of L237 and I241 pack against residues in the AS2 helix. In the Af1503-HAMP structure (24), the corresponding residues (L and V, respectively) have little surface exposure (<20 Å[2] of surface area). In the HAMP domain of Tar, I239, the residue corresponding to I241 in Tsr, is one of the least-reactive cysteine positions, indicating
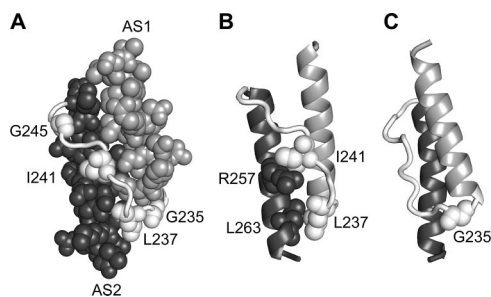
FIG. 7. Critical connector residues in the modeled Tsr-HAMP structure. For clarity, only one HAMP subunit is shown. The AS1 and AS2 helices are shaded as described in the legend of Fig. 1. All structures are oriented as shown above (A), with AS1 labeled at its N terminus and AS2 labeled at its C terminus. (A) All residues of the AS1 and AS2 helices and the functionally important residues of the connector are shown in a space-filled representation. In the modeled structure, G235 lies at the center of a tight turn (see C), and the side chains of L237 and I241 interact primarily with residues in the AS2 helix (see B). I241 is moderately exposed; L237 is more buried. G245 and neighboring residues (not shown as space filled) comprise a noncritical linker segment that packs loosely against AS2 residues oriented toward the interior of the four-helix bundle. (B) Side chain contacts between AS2 residues and functionally important connector residues. L263 lies against L237. The aliphatic portion of the R257 side chain abuts I241, but this interaction is probably not critical to Tsr function; the actual orientation of the I241 side chain may be different (see text). (C) G235 lies at a sharp turn at the end of AS1. Both of its neighboring residues (G234 and D236) have small side chains, but, unlike G235, they tolerate a variety of amino acid replacements with no loss of Tsr function.

that its side chain is probably also buried in the in vitro membrane receptor system (15, 41).

The linker segment of the connector plays a relatively nondescript role in the Tsr-HAMP structural model (Fig. 7A). Although some linker side chains lie against AS1 or AS2 residues in the Tsr-HAMP model, those interactions appear to be relatively nonspecific. Moreover, the linker residues are not conserved in different HAMP domains and appear to occupy slightly different environments in the Af1503- and Tar-HAMP structural studies. The linker residues that have the lowest surface exposures in the Af1503-HAMP structure do not correspond to the Tar-HAMP linker residues with the lowest reactivity in cysteine-scanning analyses (41). This structural variability is consistent with a role as a relatively nonspecific linker segment, as suggested by our Tsr-HAMP studies.

The four-helix bundle HAMP model predicts that connector lesions in one subunit of a heterodimer could influence the structural organization of HAMP elements in the other subunit. Although most connector lesions were recessive in heterodimer tests, a few were dominant. However, none of the connector defects acted asymmetrically, suggesting that HAMP signaling function involves structural interactions between HAMP elements in the two subunits of a receptor dimer. If the two subunits acted independently at some step, for example, in receiving asymmetric piston inputs, some HAMP defects might have shown asymmetric behavior in the heterodimer tests.

Functional interpretation of connector signaling defects. The output signaling properties of connector null mutants are

summarized in Fig. 6; we interpret them in the context of a two-state model for HAMP signaling.

Most connector mutants displayed locked (17/34) or biased (8/34) signal outputs that probably reflect changes in the relative stabilities of the CCW and CW signaling states. In principle, these sorts of lesions seem likely to destabilize one of the signaling states, but some locked mutants could have gain-of-function defects that enhance the stability of one signaling state. Biased output receptors respond to the sensory adaptation system, demonstrating that they can undergo modification changes but cannot be fully adjusted to the wild-type output setting. Locked output receptors are impervious to the sensory adaptation system; they either do not undergo modification changes or do not respond to them.

Most of the remaining connector mutants (7/34) exhibited bipolar output patterns. In the QEQE modification state, they were effectively locked in the CW mode, whereas in the presence of the sensory adaptation enzymes, they were effectively locked in the CCW mode. Evidently, these mutant receptors undergo modification changes, but we have not yet determined the nature of those changes. Bipolar receptors could conceivably arise from lesions that affect the stability of both signaling conformations, thereby altering the energy barrier between them.

Most of the locked (15/17) and bipolar (5/7) output alterations jammed Tar function in coexpression tests (Table 1 and Fig. 6), consistent with a conformationally locked condition. The jamming of heterologous receptor function is thought to occur through the formation of mixed trimers of receptor dimers, which in turn compose the signaling teams that activate and modulate the CheA kinase (2, 5). Conversely, rescuable receptor defects represent ones in which the conformation of the mutant receptor can be "repaired" by its normal partners in mixed signaling teams (5). Four connector mutants, none with locked signal output, were rescuable (Table 1). We conclude that Tsr-HAMP mutants that have jamming or rescuable phenotypes are capable of forming trimers of dimers regardless of the level of CW output that they alone can generate.

Structural interpretation of connector signaling defects. The behaviors of connector null mutants shed new light on the natures of the HAMP signaling states when considered in the context of the Tsr-HAMP structural model.

L237. Nearly all of the amino acid replacements obtained at this position had polar character and resulted in null phenotypes (Fig. 3). These replacements resulted in a wide variety of signal output patterns, suggesting that L237 plays a distinctly different signaling role from that of I241. Several replacements with hydrophobic character (C and V) retained partial or full function, but an alanine replacement was also null (Fig. 3), indicating that side chain volume, as well as hydrophobicity, is an important factor at this connector position. We suggest that L237 stabilizes both the CCW and CW signaling conformations, perhaps through an interaction with L263 in AS2 (Fig. 7B). However, this interaction is not essential for either signaling state, as evidenced by the bipolar behavior of the glycine replacement mutant (Fig. 6). Instead, L237 may serve as a conformational ratchet to control the transition rate between signal states. Some L237 replacements (e.g., A, P, S, D, and T) may destabilize one signaling state more than another, leading to biased outputs. However, some replacements (H, K, and N)

produce locked and jamming outputs that could reflect gain-of-function changes that enhance the stability of one signaling state. Finally, one replacement (Q) at L237 caused an inverted output pattern, which might reflect a change in the relative stability of the two signaling states and the way in which they respond to adaptational modifications.

I241. Glycine, charged (D, E, K, and R), and various polar (S, Q, H, and Y) amino acid replacements at this position resulted in CW-locked, CW-biased, and bipolar output patterns (Fig. 6). Conversely, residues with some hydrophobic character (P, C, V, L, M, and F), regardless of size, did not block function. These patterns suggest that the loss of a hydrophobic side chain at this position destabilizes the CCW signaling state. We conclude that the main signaling role of I241 is to stabilize the CCW signaling state. In the modeled structure, I241 interacts with R257 in the AS2 helix (Fig. 7B), but this is probably not its critical in vivo position because R257 tolerates a variety of amino acid replacements (G, S, T, Q, E, A, V, and L) with no loss of function (Q. Zhou, P. Ames, and J. S. Parkinson, unpublished data). Instead, we suggest that the I241 side chain may stabilize the CCW HAMP conformation by packing into the groove between the AS1 and AS2 helices, thereby influencing their relative motions or orientation.

G235. Null lesions at this residue caused strong jamming defects and mainly locked or bipolar output patterns (Fig. 6). These behaviors indicate that G235 is probably a key player in effecting signaling-related conformational changes in the HAMP domain. Side chain volume appears to be an important factor at this position because medium-sized residues of either hydrophobic (C, L, and M) or polar (Q and H) character locked output in the CCW mode. These mutant receptors exhibited functional dominance in heterodimer tests, consistent with strong gain-of-function defects. Similarly, acidic residues (D and E) at this position locked output in the CW mode, and those defects were partially dominant in heterodimer tests. Acidic replacements at G235 might have a unique influence on HAMP conformation and, consequently, on the output state through charge interactions with the adjacent D236 residue. Thus, depending on their volume and chemical properties, side chains of intermediate size may stabilize different backbone geometries, effectively locking HAMP in the CCW or CW signaling conformation. In contrast, very small (A, S, and N) and very large (F, K, R, and Y) residues allowed some Tsr function; a tryptophan replacement mutant retained full function (Fig. 3). Small residues probably allow some function because they have few constraining side chain interactions with neighboring residues. Conversely, large residues may allow function because their side chain orientation at the turn is fully constrained. Overall, these mutant patterns are consistent with the turn location of G235 in the modeled Tsr-HAMP structure (Fig. 7C).

Proline replacements, which would be expected to reduce backbone flexibility, abrogated function at all three connector turn residues (G234, G235, and D236) but with different signaling consequences (Fig. 6). The G234P receptor exhibited bipolar output, the G235P mutant had an unbiased output pattern, and the D236P mutant was locked in the CW mode. Evidently, backbone motions in the turn residues influence the switching rates between HAMP signaling conformations. In

the context of the Tsr-HAMP structural model, the signaling properties of G235 lesions and of proline replacements at the other turn residues could reflect structural perturbations of L237, the putative conformational ratchet for signal state switches.

Nature of HAMP signaling states. Our analysis of connector lesions makes a strong case that the modeled Tsr-HAMP structure corresponds closely to one of the in vivo HAMP signaling conformations. What might the alternative signaling conformation be? If we assume that our mutant connector proteins have near-native structures, as suggested by their normal intracellular stabilities, then it seems likely that the alternative HAMP signaling state is not very different from the modeled structure. We found, for example, that modest differences in side chain volume and chemical properties at critical connector residues could shift HAMP output states. Moreover, many of the mutant outputs (biased, bipolar, or inverted) could be shifted to the alternate signaling state by the sensory adaptation system, behavior that is also consistent with relatively modest conformational changes. Thus, we conclude that the two native HAMP signaling conformations have similar structures. This view argues against dramatic rearrangements of the HAMP structural elements upon signal state changes, for example, a reversible association of AS1 with the cytoplasmic membrane (46). Instead, the two HAMP output conformations may differ by shifts in helix packing, as proposed in the gearbox model (24), or by changes in HAMP structural stability that in turn influence the dynamic motions or packing arrangements of the methylation and kinase control helices.

Implications for HAMP domains in other signaling proteins. Owing to the lack of a compensatory sensory adaptation system, HAMP function in non-MCP signaling proteins should be more sensitive to mutation than it is in Tsr. Thus, HAMP residues that are relatively unimportant in Tsr may seem much more critical in other signaling proteins. Although only a few connector mutations in other HAMP-containing proteins have been characterized, this appears to be the case for NarX, a transmembrane sensor kinase, and for Aer, a transducer for aerotaxis. Two connector residues identified by regulatory mutations in NarX, G205R and N207I (7, 26), correspond to linker residues of Tsr (G245 and N247) that are not critical for function, although replacements at Tsr-G245 do compromise function to some extent. Although Aer has an MCP-like signaling domain, it lacks methylation sites and is not dependent on the MCP sensory adaptation enzymes (10). Amino acid replacements at Aer connector residues N228, V230, R235, and D237 disrupt function (14, 30), whereas changes at the corresponding Tsr residues (V238, P240, G245, and N247) do not.

This study is the first extensive analysis of HAMP mutants in any signaling protein, and despite the adaptation capabilities of MCPs, our Tsr findings should be relevant to other HAMP-containing signaling proteins. For example, a connector lesion in NarX (R195C) that impairs the induction of a *narG-lacZ* reporter (7), implying a kinase-off signaling condition, corresponds to Tsr-G235C, which exhibits CCW-locked (i.e., kinase-off) output. We expect that further characterization of Tsr-HAMP mutants will provide general insights into the structure and function of HAMP domains in bacterial signaling proteins.

REFERENCES

1. **Alexander, R. P., and I. B. Zhulin.** 2007. Evolutionary genomics reveals conserved structural determinants of signaling and adaptation in microbial chemoreceptors. Proc. Natl. Acad. Sci. USA **104:**2885–2890.
2. **Ames, P., and J. S. Parkinson.** 2006. Conformational suppression of inter-receptor signaling defects. Proc. Natl. Acad. Sci. USA **103:**9292–9297.
3. **Ames, P., and J. S. Parkinson.** 1994. Constitutively signaling fragments of Tsr, the *Escherichia coli* serine chemoreceptor. J. Bacteriol. **176:**6340–6348.
4. **Ames, P., and J. S. Parkinson.** 1988. Transmembrane signaling by bacterial chemoreceptors: *E. coli* transducers with locked signal output. Cell **55:**817–826.
5. **Ames, P., C. A. Studdert, R. H. Reiser, and J. S. Parkinson.** 2002. Collaborative signaling by mixed chemoreceptor teams in *Escherichia coli*. Proc. Natl. Acad. Sci. USA **99:**7060–7065.
6. **Appleman, J. A., L. L. Chen, and V. Stewart.** 2003. Probing conservation of HAMP linker structure and signal transduction mechanism through analysis of hybrid sensor kinases. J. Bacteriol. **185:**4872–4882.
7. **Appleman, J. A., and V. Stewart.** 2003. Mutational analysis of a conserved signal-transducing element: the HAMP linker of the *Escherichia coli* nitrate sensor NarX. J. Bacteriol. **185:**89–97.
8. **Aravind, L., and C. P. Ponting.** 1999. The cytoplasmic helical linker domain of receptor histidine kinase and methyl-accepting proteins is common to many prokaryotic signalling proteins. FEMS Microbiol. Lett. **176:**111–116.
9. **Baumgartner, J. W., C. Kim, R. R. Brissette, M. Inouye, C. Park, and G. L. Hazelbauer.** 1994. Transmembrane signalling by a hybrid protein: communication from the domain of chemoreceptor Trg that recognizes sugar-binding proteins to kinase/phosphatase domain of osmosensor EnvZ. J. Bacteriol. **176:**1157–1163.
10. **Bibikov, S. I., A. C. Miller, K. K. Gosink, and J. S. Parkinson.** 2004. Methylation-independent aerotaxis mediated by the *Escherichia coli* Aer protein. J. Bacteriol. **186:**3730–3737.
11. **Boldog, T., S. Grimme, M. Li, S. G. Sligar, and G. L. Hazelbauer.** 2006. Nanodiscs separate chemoreceptor oligomeric states and reveal their signaling properties. Proc. Natl. Acad. Sci. USA **103:**11509–11514.
12. **Bolivar, F., R. Rodriguez, P. J. Greene, M. C. Betlach, H. L. Heyneker, and H. W. Boyer.** 1977. Construction and characterization of new cloning vehicles. Gene **2:**95–113.
13. **Bornhorst, J. A., and J. J. Falke.** 2001. Evidence that both ligand binding and covalent adaptation drive a two-state equilibrium in the aspartate receptor signaling complex. J. Gen. Physiol. **118:**693–710.
14. **Buron-Barral, M., K. K. Gosink, and J. S. Parkinson.** 2006. Loss- and gain-of-function mutations in the F1-HAMP region of the *Escherichia coli* aerotaxis transducer Aer. J. Bacteriol. **188:**3477–3486.
15. **Butler, S. L., and J. J. Falke.** 1998. Cysteine and disulfide scanning reveals two amphiphilic helices in the linker region of the aspartate chemoreceptor. Biochem. **37:**10746–10756.
16. **Chang, A. C. Y., and S. N. Cohen.** 1978. Construction and characterization of amplifiable multicopy DNA cloning vehicles derived from the p15A cryptic miniplasmid. J. Bacteriol. **134:**1141–1156.
17. **Cochran, A. G., and P. S. Kim.** 1996. Imitation of *Escherichia coli* aspartate receptor signaling in engineered dimers of the cytoplasmic domain. Science **271:**1113–1116.
18. **Falke, J. J., and G. L. Hazelbauer.** 2001. Transmembrane signaling in bacterial chemoreceptors. Trends Biochem. Sci. **26:**257–265.
19. **Francis, N. R., M. N. Levit, T. R. Shaikh, L. A. Melanson, J. B. Stock, and D. J. DeRosier.** 2002. Subunit organization in a soluble complex of Tar, CheW, and CheA by electron microscopy. J. Biol. Chem. **277:**36755–36759.
20. **Francis, N. R., P. M. Wolanin, J. B. Stock, D. J. Derosier, and D. R. Thomas.** 2004. Three-dimensional structure and organization of a receptor/signaling complex. Proc. Natl. Acad. Sci. USA **101:**17480–17485.
21. **Gosink, K. K., M. Buron-Barral, and J. S. Parkinson.** 2006. Signaling interactions between the aerotaxis transducer Aer and heterologous chemoreceptors in *Escherichia coli*. J. Bacteriol. **188:**3487–3493.
22. **Greer-Phillips, S. E., G. Alexandre, B. L. Taylor, and I. B. Zhulin.** 2003. Aer and Tsr guide *Escherichia coli* in spatial gradients of oxidizable substrates. Microbiology **149:**2661–2667.
23. **Hazelbauer, G. L., J. J. Falke, and J. S. Parkinson.** 2008. Bacterial chemoreceptors: high-performance signaling in networked arrays. Trends Biochem. Sci. **33:**9–19.
24. **Hulko, M., F. Berndt, M. Gruber, J. U. Linder, V. Truffault, A. Schultz, J. Martin, J. E. Schultz, A. N. Lupas, and M. Coles.** 2006. The HAMP domain structure implies helix rotation in transmembrane signaling. Cell **126:**929–940.
25. **Jung, K. H., E. N. Spudich, V. D. Trivedi, and J. L. Spudich.** 2001. An archaeal photosignal-transducing module mediates phototaxis in *Escherichia coli*. J. Bacteriol. **183:**6365–6371.
26. **Kalman, L. V., and R. P. Gunsalus.** 1990. Nitrate- and molybdenum-independent signal transduction mutations in *narX* that alter regulation of anaerobic respiratory genes in *Escherichia coli*. J. Bacteriol. **172:**7049–7056.
27. **Kristich, C. J., and G. W. Ordal.** 2004. Analysis of chimeric chemoreceptors in *Bacillus subtilis* reveals a role for CheD in the function of the McpC HAMP domain. J. Bacteriol. **186:**5950–5955.
28. **Lai, W. C., B. D. Beel, and G. L. Hazelbauer.** 2006. Adaptational modification and ligand occupancy have opposite effects on positioning of the transmembrane signalling helix of a chemoreceptor. Mol. Microbiol. **61:**1081–1090.
29. **Liu, J. D., and J. S. Parkinson.** 1989. Role of CheW protein in coupling membrane receptors to the intracellular signaling system of bacterial chemotaxis. Proc. Natl. Acad. Sci. USA **86:**8703–8707.
30. **Ma, Q., M. S. Johnson, and B. L. Taylor.** 2005. Genetic analysis of the HAMP domain of the Aer aerotaxis sensor localizes flavin adenine dinucleotide-binding determinants to the AS-2 helix. J. Bacteriol. **187:**193–201.
31. **Montefusco, D. J., A. L. Shrout, T. Y. Besschetnova, and R. M. Weis.** 2007. Formation and activity of template-assembled receptor signaling complexes. Langmuir **23:**3280–3289.
32. **Parkinson, J. S.** 1976. *cheA*, *cheB*, and *cheC* genes of *Escherichia coli* and their role in chemotaxis. J. Bacteriol. **126:**758–770.
33. **Parkinson, J. S., P. Ames, and C. A. Studdert.** 2005. Collaborative signaling by bacterial chemoreceptors. Curr. Opin. Microbiol. **8:**116–121.
34. **Parkinson, J. S., and S. E. Houts.** 1982. Isolation and behavior of *Escherichia coli* deletion mutants lacking chemotaxis functions. J. Bacteriol. **151:**106–113.
35. **Rebbapragada, A., M. S. Johnson, G. P. Harding, A. J. Zuccarelli, H. M. Fletcher, I. B. Zhulin, and B. L. Taylor.** 1997. The Aer protein and the serine chemoreceptor Tsr independently sense intracellular energy levels and transduce oxygen, redox, and energy signals for *Escherichia coli* behavior. Proc. Natl. Acad. Sci. USA **94:**10541–10546.
36. **Schwede, T., J. Kopp, N. Guex, and M. C. Peitsch.** 2003. SWISS-MODEL: an automated protein homology-modeling server. Nucleic Acids Res. **31:**3381–3385.
37. **Shrout, A. L., D. J. Montefusco, and R. M. Weis.** 2003. Template-directed assembly of receptor signaling complexes. Biochemistry **42:**13379–13385.
38. **Studdert, C. A., and J. S. Parkinson.** 2004. Crosslinking snapshots of bacterial chemoreceptor squads. Proc. Natl. Acad. Sci. USA **101:**2117–2122.
39. **Studdert, C. A., and J. S. Parkinson.** 2005. Insights into the organization and dynamics of bacterial chemoreceptor clusters through in vivo crosslinking studies. Proc. Natl. Acad. Sci. USA **102:**15623–15628.
40. **Surette, M. G., and J. B. Stock.** 1996. Role of alpha-helical coiled-coil interactions in receptor dimerization, signaling, and adaptation during bacterial chemotaxis. J. Biol. Chem. **271:**17966–17973.
41. **Swain, K. E., and J. J. Falke.** 2007. Structure of the conserved HAMP domain in an intact, membrane-bound chemoreceptor: a disulfide mapping study. Biochemistry **46:**13684–13695.
42. **Umemura, T., Y. Matsumoto, K. Ohnishi, M. Homma, and I. Kawagishi.** 2002. Sensing of cytoplasmic pH by bacterial chemoreceptors involves the linker region that connects the membrane-spanning and the signal-modulating helices. J. Biol. Chem. **277:**1593–1598.
43. **Utsumi, R., R. E. Brissette, A. Rampersaud, S. A. Forst, K. Oosawa, and M. Inouye.** 1989. Activation of bacterial porin gene expression by a chimeric signal transducer in response to aspartate. Science **245:**1246–1249.
44. **Ward, S. M., A. Delgado, R. P. Gunsalus, and M. D. Manson.** 2002. A NarX-Tar chimera mediates repellent chemotaxis to nitrate and nitrite. Mol. Microbiol. **44:**709–719.
45. **Watts, K. J., M. S. Johnson, and B. L. Taylor.** 2008. Structure-function relationships in the HAMP and proximal signaling domains of the aerotaxis receptor Aer. J. Bacteriol. **190:**2118–2127.
46. **Williams, S. B., and V. Stewart.** 1999. Functional similarities among two-component sensors and methyl-accepting chemotaxis proteins suggest a role for linker region amphipathic helices in transmembrane signal transduction. Mol. Microbiol. **33:**1093–1102.
47. **Wolanin, P. M., M. D. Baker, N. R. Francis, D. R. Thomas, D. J. DeRosier, and J. B. Stock.** 2006. Self-assembly of receptor/signaling complexes in bacterial chemotaxis. Proc. Natl. Acad. Sci. USA **103:**14313–14318.
48. **Yen, K. M.** 1991. Construction of cloning cartridges for development of expression vectors in gram-negative bacteria. J. Bacteriol. **173:**5328–5335.
49. **Zhu, Y., and M. Inouye.** 2003. Analysis of the role of the EnvZ linker region in signal transduction using a chimeric Tar/EnvZ receptor protein, Tez1. J. Biol. Chem. **278:**22812–22819.